Title
Integrated intravital microscopy and mathematical modeling to optimize nanotherapeutics delivery to tumors

Journal
AIP Advances, 2(1)

ISSN
21583226

Authors
van de Ven, Anne L
Wu, Min
Lowengrub, John
et al.

Publication Date
2012

DOI
10.1063/1.3699060

Integrated intravital microscopy and mathematical modeling to optimize nanotherapeutics delivery to tumors

Anne L. van de Ven,[1,a] Min Wu,[2] John Lowengrub,[2] Steven R. McDougall,[3] Mark A. J. Chaplain,[4] Vittorio Cristini,[5,6] Mauro Ferrari,[1] and Hermann B. Frieboes[7,8,a]

[1]*Department of Nanomedicine, The Methodist Hospital Research Institute, 6670 Bertner Avenue, Houston, Texas, 77030, USA*
[2]*Department of Mathematics, University of California, Irvine, California, 92697, USA*
[3]*Institute of Petroleum Engineering, Heriot-Watt University, Edinburgh, Scotland, UK*
[4]*Division of Mathematics, University of Dundee, Dundee, Scotland, UK*
[5]*Department of Pathology. University of New Mexico, Albuquerque, New Mexico, 87106, USA*
[6]*Chemical Engineering, University of New Mexico, Albuquerque, New Mexico, 87106, USA*
[7]*Department of Bioengineering, University of Louisville, 419 Lutz Hall, Louisville, Kentucky 40208, USA*
[8]*James Graham Brown Cancer Center, University of Louisville, 419 Lutz Hall, Louisville, Kentucky 40208, USA*

(Received 6 September 2011; accepted 5 November 2011; published online 22 March 2012)

Inefficient vascularization hinders the optimal transport of cell nutrients, oxygen, and drugs to cancer cells in solid tumors. Gradients of these substances maintain a heterogeneous cell-scale microenvironment through which drugs and their carriers must travel, significantly limiting optimal drug exposure. In this study, we integrate intravital microscopy with a mathematical model of cancer to evaluate the behavior of nanoparticle-based drug delivery systems designed to circumvent biophysical barriers. We simulate the effect of doxorubicin delivered via porous 1000 x 400 nm plateloid silicon particles to a solid tumor characterized by a realistic vasculature, and vary the parameters to determine how much drug per particle and how many particles need to be released within the vasculature in order to achieve remission of the tumor. We envision that this work will contribute to the development of quantitative measures of nanoparticle design and drug loading in order to optimize cancer treatment via nanotherapeutics. [http://dx.doi.org/10.1063/1.3699060]

I. INTRODUCTION

The importance of understanding physical phenomena occurring within cancer lesions has recently been reviewed,[1] with specific reference to the transport and delivery of systemically administered therapeutics. The term "Transport OncoPhysics" has been introduced for the study of such multi-scale transport phenomena.[2] A fundamental observation of Transport OncoPhysics is that the biological distribution of systemically injected agents is largely a function of their ability to negotiate a sequential multitude of biophysical barriers. These biophysical barriers present a formidable obstacle to nanoparticle-based drug delivery.[2–4] To reach a tumor, nanoparticles circulating in the vasculature must avoid uptake by the reticulo-endothelial system (RES), evade immune system cells, and retain structural integrity until reaching their target. Within the tumor itself, optimal transport of nanotherapeutics to the cancer cells is hindered by inefficient tumor vascularization and adverse interstitial fluid pressure.[5–7] Gradients of cell nutrients, oxygen, and other cell substrates, as

[a]Authors to whom correspondence should be addressed. Electronic mail: avandeven@tmhs.org, Phone: 713-441-7449, Fax: 713-441-7438. Electronic mail: hbfrie01@louisville.edu, Phone: 502-852-3302, Fax: 502-852-6806.

well as drugs, help maintain a heterogeneous cellular microenvironment that can impact treatment efficacy.

Modeling the intratumoral behavior of nanotherapeutics depends on an accurate physical description of the tumor microenvironment, the parameters of which are derived from cancer biology. This modeling aims to predict actual tissue response by representing the tumor as a mass governed by physical laws such as mass, momentum, and energy balance. Extensive work in modeling tumor growth and vascularization has occurred in the past two decades (see recent reviews[8–16]). Specialized models have been developed to study angiogenesis and vascular flow,[17–22] drug delivery and response,[5–7,23–25] as well as the role of the three-dimensional tumor microenvironment.[26–33] Abstracting the main components of this physical formulation into a mathematical model enables implementation of a computational system that aims to predict treatment response of real tumors. However, it is difficult to model from the nanoparticle (10^{-9} m) to the tumor (10^{-3} m) scale, not only because tissue behaves very differently at each scale, but because of the prohibitively high computational cost associated with modeling length scales over six orders of magnitude for significant periods of biological time. It is also challenging for models to remain biologically relevant while retaining the capability to numerically solve for concrete results. Consequently, there are few physical models incorporating nanotherapeutics with solid tumor growth, especially taking into account the complex multi-dimensional tumor microenvironment.

Nanoparticle-based drug delivery and treatment response in a two-dimensional vascularized tumor model was first studied by Sinek *et al.*[5] in a model based on work by.[17,34] This study demonstrated that the potential efficacy of nanoparticle-based therapeutics is primarily determined by physical transport limitations. Two kinds of particles were considered: very small (e.g., 1-10 nm) nanoparticles that extravasate from the tumor vasculature and diffuse through the interstitium and larger (e.g., $>$100 nm) non-diffusing particles that remain at their point of extravasation from the vasculature and function as a constant source of drug. In both cases, the nanoparticle localization was assumed to be associated with fenestrations in the tumor vasculature. By acting as point sources of drug, the nanoparticles produced larger and more uniform drug concentrations over longer periods of time compared to traditional free-drug administration. However, the results also showed that drugs released from nanoparticles would suffer from the same fundamental transport limitations as free-drug administration. Competition between vasculature density, which favors nutrient and nanoparticle extravasation, and intratumoral pressure, which may oppose it, typically results in non-uniform delivery. Heterogeneities in oxygen, nutrient, and drug diffusion within the tumor interstitium would further contribute to this non-uniformity.

The study of nanoparticle-based drug delivery requires an understanding of tumor vascularization and the unique features of intratumoral blood flow. Interactions between blood flow and the changing tumor vasculature may be examined by coupling an updated version of the continuum tumor model described above[33,34] with a more elaborate model of tumor-induced angiogenesis.[17–19] This multi-scale model, first described in Macklin *et al.*,[22] incorporates angiogenic factors and metabolic substrates released by the tumor cells and neovasculature, respectively. Vascular fluid flow, and hence transport of cell substrates, is impeded by hydrostatic pressure from the growing tumor, which in turn constricts the neovasculature, leading to altered shear stresses and flow patterns. The vascular network and tumor growth are coupled to an extracellular matrix (ECM) in order to simulate the role of ECM degradation during endothelial and tumor cell migration.

In recent work by Wu *et al.*,[35] we have extended this modeling framework to incorporate interstitial pressure and flow, a lymphatic system to model fluid drainage, and blood vessel leakage. The resulting system provides a more realistic model to simulate the flow and distribution of nanoparticles within the tumor vasculature. Here, we integrate intravital microscopy data to evaluate the behavior of nanoparticle-based drug delivery systems designed to circumvent biophysical barriers. We simulate the effect of doxorubicin delivered via porous silicon particles to a solid tumor in order to determine how much drug per particle and how many particles need to be released within the vasculature in order to achieve remission of the tumor. Implications for particle design and optimization are discussed, as well as potential future applications and extensions of the model.

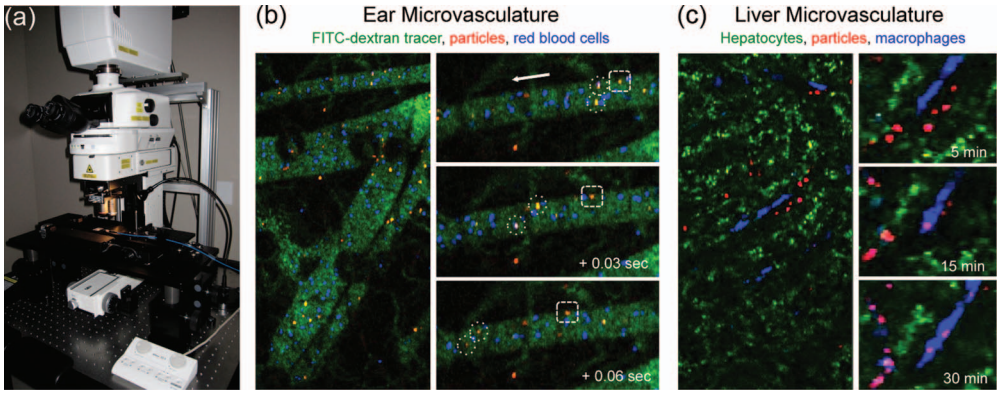

FIG. 1. Intravital microscopy (IVM) for the tracking of individual nanoparticles in blood flow. a) Images are acquired using an upright Nikon laser scanning confocal microscope equipped with a resonant scanner for high-speed imaging. Both non-invasive and acute tissue preparations can be visualized with high spatial and temporal resolution. b) Dynamics of individual 1000 x 400 nm plateloid silicon particles (shown in red) imaged non-invasively in the microvasculature of the mouse ear. The circles indicate fast-moving particles in the center of the flow; the box indicates a relatively slow-moving particle near the vessel wall (enhanced online) [URL: http://dx.doi.org/10.1063/1.3699060.1] . c) Time-dependent uptake of porous silicon particles by macrophages residing in the liver of a wild-type mouse, as measured from the time of injection.

II. DYNAMIC INTRAVITAL MICROSCOPY

Intravital microscopy (IVM) can be used to collect dynamic, quantitative information *in vivo* with cellular and/or subcellular resolution. We have developed techniques that allow the dynamics of individual nanoparticles to be monitored and quantified in real-time in live small animals.[36] A variety of organs can be studied acutely or longitudinally via surgical manipulations, including the skin, liver, spleen, and solid tumors by coupling advanced image-processing algorithms to high-resolution microscopes with optical sectioning capabilities. Nanoparticle accumulation in blood vessels, tumor fenestrations, and specific cells of interest can be dynamically visualized with the selection of appropriate vital dyes or the use of transgenic animal strains. FIG. 1 (enhanced) highlights sample time-lapse images of plateloid silicon particles (1000 nm diameter x 400 nm thickness) in the ear and liver of healthy wild-type C57 mice. These particles were selected for their favorable biodistribution profile,[37] ability to rapidly and effectively accumulate in tumors,[36] and lack of toxicity *in vitro*[38] and *in vivo*.[39] A video of single particle dynamics may be found online.

The delivery of nanotherapeutics to solid tumors is a relatively inefficient process, with generally less than 1% per unit mass of the target organ reaching the intratumoral space. IVM can be used to determine how many particles reach a tumor and how quickly they get there, opening opportunities for studying and optimizing nanoparticle delivery in a systematic manner. We are currently using IVM to investigate the delivery of porous silicon particles to the microvasculature of solid tumors. Bare porous silicon particles have a relatively short half-life in circulation and predominately accumulate in tumors in the first few minutes after injection. These behaviors can be quantified *in vivo* by optically monitoring particle flow through a small region of tumor ($\sim$0.1 mm^3). To account for region-specific heterogeneities in particle accumulation, the automated image acquisition may be programmed to rapidly sample multiple fields of view in an iterative manner. FIG. 2 shows typical circulation and accumulation data measured for a single mouse bearing a subcutaneous melanoma xenograft. We find that particle accumulation trends are highly reproducible from animal to animal within a single tumor model,[36] supporting the use of IVM for quantifying particle delivery *in vivo*.

The overall size of these particles makes it likely that they become lodged within the tumor microvasculature, rather than extravasating out of the tumor fenestrations. As such, they have the potential to serve as localized intravascular drug delivery depots that can release multiple smaller nanoparticles in close proximity to the tumor cells, a concept first proposed by our laboratory[2] and demonstrated *in vivo* by Tanaka *et al.*[39] For this strategy to succeed clinically, it is important to determine how many particles are needed to achieve a therapeutic benefit, to define the role of tumor

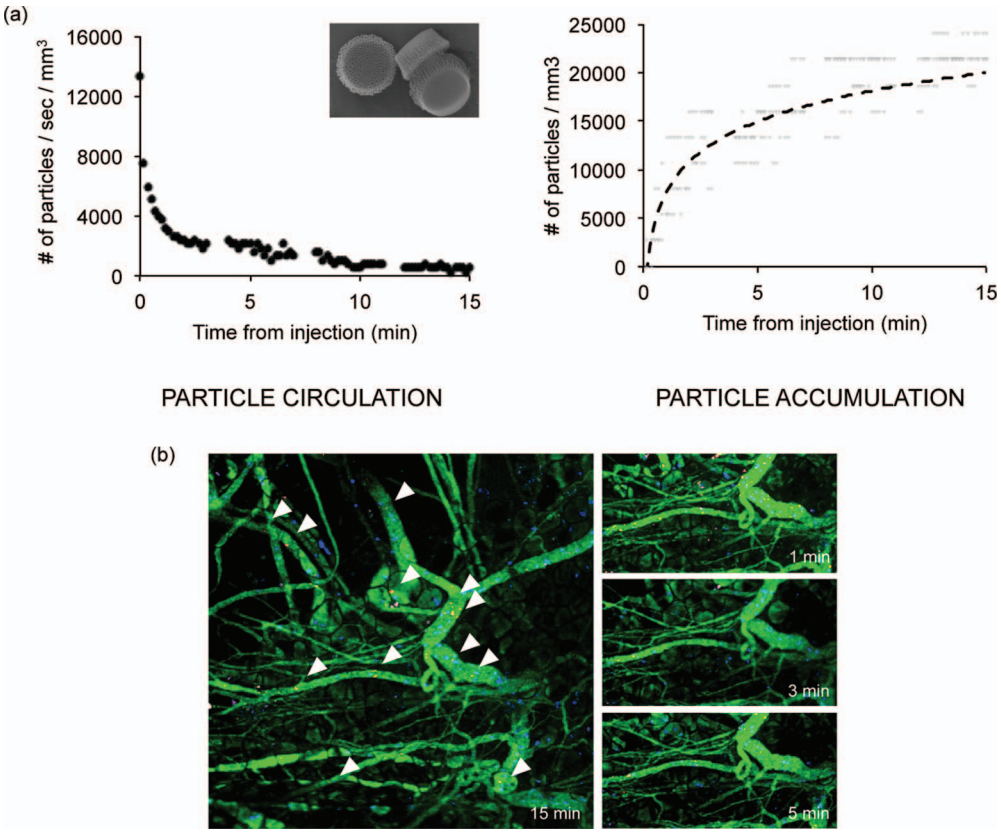

FIG. 2. Intratumoral circulation and accumulation of porous 1000 x 400nm plateloid silicon particles, as measured by IVM. Melanoma xenografts were grown in the flank to a size of 200mm^3, surgically exposed, and imaged in real-time following particle injection. a) The number of moving (left) and static (right) particles per field-of-view (400×400×6 μm) were quantified as a function of time to yield the circulation and accumulation curves. Raw accumulation data is shown in gray; the fluctuations in the data reflect images collected in multiple regions and multiple focal planes within the same tumor. Inset, SEM image of porous 1000 x 400 nm plateloid silicon particles. b) IVM images of plateloid particle accumulation in melanoma. One minute after injection, both adherent and circulating particles (red) are observed within the FITC-dextran labeled vasculature (green). As the number of circulating particles drops, more and more adherent particles are observed. The arrows indicate several adherent particles 15 minutes after injection.

vascularization in particle transport and accumulation, and to determine how the intratumoral spatial distribution of particles influences their efficacy.

III. COMPUTATIONAL MODELING

The model simulates the transport and accumulation of nanoparticles within the microvasculature of a solid tumor. The particles are assumed to steadily release a chemotherapeutic drug, modeled here as doxorubicin, into the surrounding tissue for a period of 4 days, and then exhaust the drug supply. The drug diffuses through the interstitial space and is taken up by proliferating tumor cells, resulting in apoptosis once a certain uptake threshold is reached. The model parameters are initialized using biologically relevant values as detailed in Wu *et al.*[35] FIG. 3 shows the simulated tumor and associated microvasculature at the start of therapy.

In our model, systemically injected nanoparticles loaded with doxorubicin enter via the tumor vasculature and become lodged along the vessel walls in or near tumor fenestrations. This phenomenon has been observed using IVM and scanning electron microscopy (van de Ven, submitted). Nanoporous silicon particles may be engineered to release drugs over the course of hours[40] to days[41] by tailoring silicon degradation kinetics.[42] Here we treat the adherent particles as point sources of doxorubicin, which is assumed to be released in a constant manner over a period of

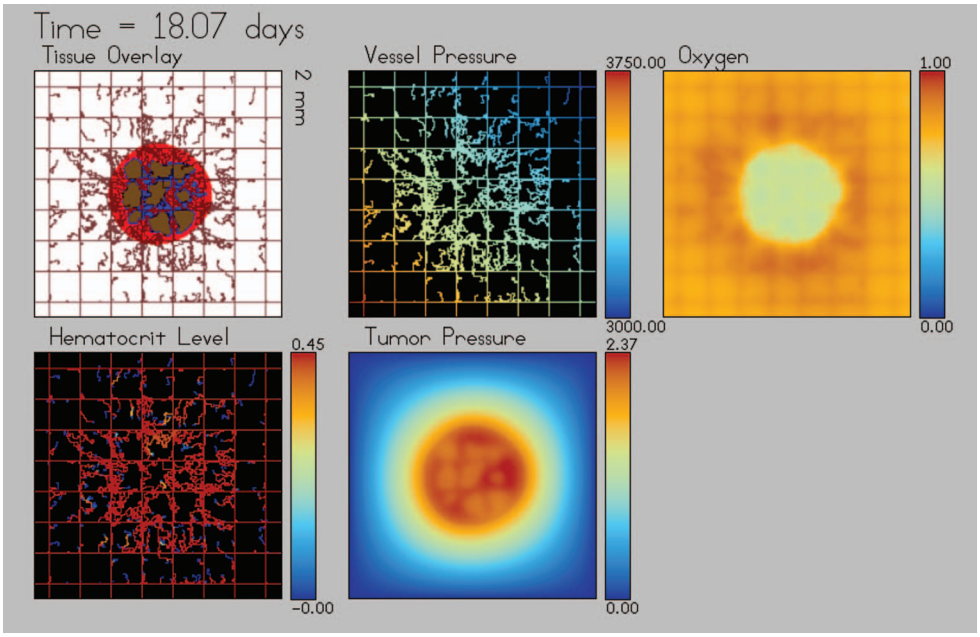

FIG. 3. Simulated tumor at the start of therapy. Nanoparticles are assumed to be convected through the vasculature and lodge preferentially in the tumor neovasculature, from where the drug will be released into the tumor tissue. Clockwise from top: Tissue in a 2x2mm area: tumor with viable tissue in red, hypoxic in blue, and necrotic in brown, is shown with the pre-existing vasculature (brown rectangular grid) as well as the neovasculature (irregular brown lines) originating in response to the net release of pro-angiogenic factors from the tumor hypoxic regions; Vessel pressure (Pa) is assumed to establish a gradient across the capillary bed from high (bottom left corner of frame) to low (upper right corner); Oxygen distribution as a fraction of the maximum in the vasculature is heterogeneous based on the uptake by the proliferating cells within the tumor region and the delivery by the neovascular network; Hematocrit level (as fraction of blood volume) shows flowing blood concentration; Tumor pressure (non-dimensionalized as in[22]) is highest in the proliferating viable tumor regions.

four days (see Methods). We further estimate the uptake rate of doxorubicin to range from 10^{-4} to 10^{-5} sec^{-1},[7] whereas the oxygen uptake rate has been measured to be $\sim 10^{-1}$ sec^{-1}.[43] FIG. 4 shows the tumor inhibition and drug distribution calculated for various levels of drug concentration $\bar{C}_D$, a non-dimensionalized parameter that represents the initial amount of drug loaded into the particles at the tumor site. We observe that after 4 days of treatment, the proportion viable (red) and hypoxic (blue) tissue is reduced, leading to an overall reduction in tumor volume. As expected, the case of highest initial drug concentration ($\bar{C}_D = 5$) leads to the most tumor regression (FIG. 5). Changes in oxygen distribution and tumor pressure are observed, concomitant with cell apoptosis and an overall decrease in cell proliferation.

Interestingly, the model predicts that cell death resulting from treatment is not linearly proportional to the concentration of drug delivered by the nanoparticles. Instead, a saturation phenomenon occurs in which increasing the amount of drug leads to a correspondingly smaller increase in the death effect. As a result, the relationship between tumor regression (as measured by the tumor radius) and the parameter $\bar{C}_D$is nonlinear. This is illustrated in FIG. 6(a). This saturation effect is well known from previous studies (e.g., see[44]), where a linear increase in drug concentration does not necessarily correspond to a linear increase in the death effect. One reason for this phenomenon is that cell death and removal is a relatively slow process (typically 6 to 12 hours), while the penetration of the drug itself through the tissue follows an exponential decay due to the transport barriers imposed by diffusion and tissue density.[7] This has some interesting implications for nanoparticle-based delivery, which are discussed in further detail below.

In order to elucidate the tumor response to doxorubicin treatment, one can define the concentration of drug required to inhibit growth of half of the tumor mass, called the "IC_{50}" (half maximal inhibitory concentration). This was measured to be on the order of ≤ 170 μM for BL16-B6 murine melanoma cells *in vitro*.[45] This IC_{50} is of similar magnitude to other cancer cells lines that are

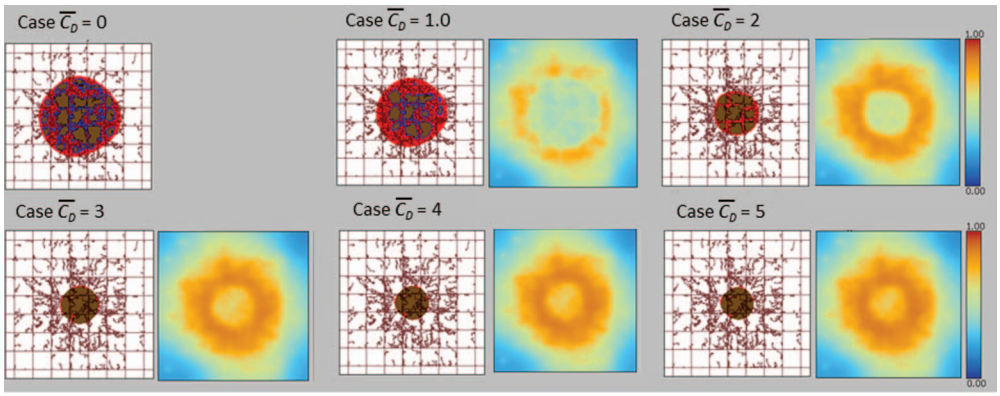

FIG. 4. Tumor inhibition simulated after 4 days of doxorubicin release from nanoparticles lodged in the tumor neovasculature for various values of the initial drug concentration $\bar{C}_D$ at the tumor site (same color scheme as FIG. 3). This parameter provides a means to calculate the amount of drug necessary to achieve a particular tumor inhibition (see Methods). Tumor panels (same color scheme as FIG. 3) are shown with corresponding drug distributions (orange to blue color) as a fraction of the maximum value in the vasculature.

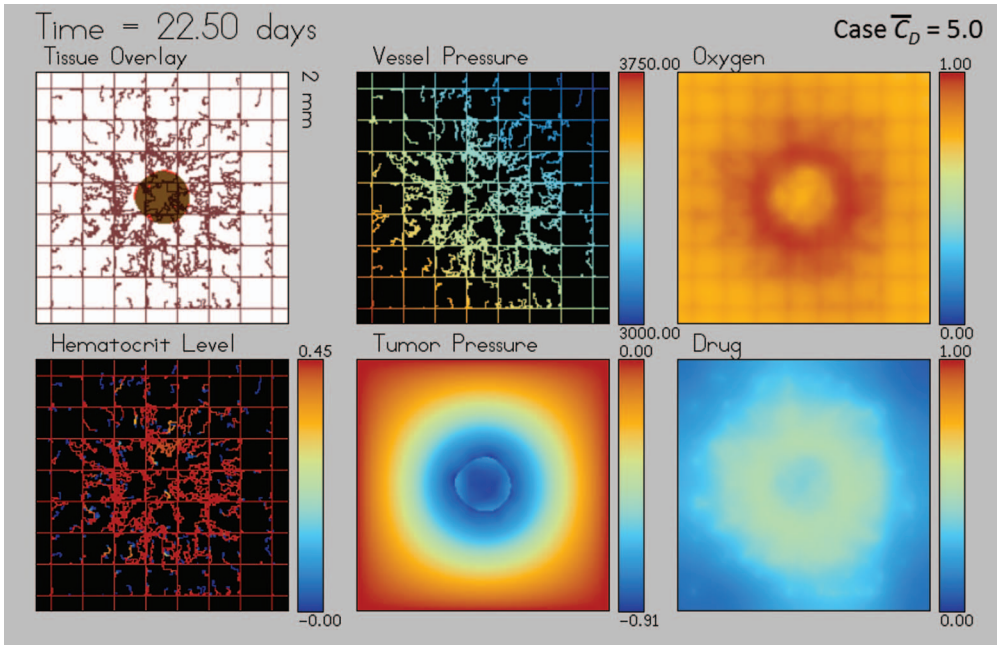

FIG. 5. Examination of the case simulating highest initial drug concentration ($\bar{C}_D = 5.0$) at the tumor site a half day after the end of treatment (day 4.5) shows that the oxygen concentration (top/right panel) becomes more homogeneous than in the initial tumor (FIG. 3) due to massive apoptosis and concomitant reduction in cell proliferation, which are reflected in the negative tumor pressure. Any remaining drug (bottom/right panel) is rapidly dissipating through the interstitium (in contrast to FIG. 4).

considered sensitive to doxorubicin. Accordingly, we estimate that the IC_{50} for BL16 cells *in vivo* could fall in the range of 10 to 100 μM, assuming that these idealized *in vitro* conditions approximate a vascularized tissue *in vivo*. We can assign values to the non-dimensionalized parameter $\bar{C}_D$ by relating these experimental observations to the simulated results. In Fig. 6(b) we plot the tumor radius at the end of treatment as a fraction of the untreated control for different values of initial drug concentration $\bar{C}_D$, showing that $\bar{C}_D \geq 1.2$ would yield ~50% or greater tumor inhibition. If we assume that the concentration $\bar{C}_D$=1.2 is of similar magnitude as the IC_{50} of BL16 cells *in vitro*,

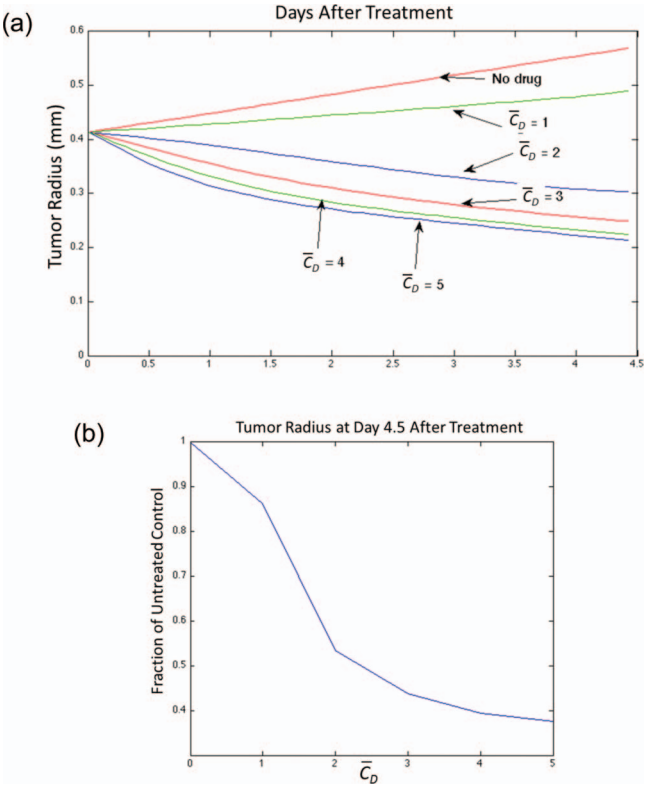

FIG. 6. a) Comparison of tumor inhibition based on different values of initial drug concentration $\bar{C}_D$ at the tumor site, showing a nonlinear relationship between tumor regression and drug concentration. Note that the case $\bar{C}_D$=1 may be insufficient to achieve tumor regression. b) Plot of tumor size at the end of treatment as a function of initial drug concentration, showing that values of initial drug concentration $\bar{C}_D > 1.2$ would lead to a tumor volume reduction of 50% or higher (i.e., the radius needs to shrink by at least 21%).

we estimate that one would need to load 0.5 - 50 mg doxorubicin in ∼10 billion particles to reach sufficient intratumoral concentrations (discussed in further detail below).

IV. DISCUSSION

The clinical outcome of nanotherapeutics can be predicted in a quantitative manner. Here we modeled nanoparticle-based drug delivery in terms of diffusion-driven intra-tumoral heterogeneity. Model parameters, when calibrated to experimental data, provide realistic numbers describing biological behaviors. When these simulations are paired with intravital microscopy data, several interesting points emerge regarding particle loading, delivery, and optimization. In our melanoma animal model, we are able to reproducibly deliver ∼14,000 – 18,000 particles/mm^3. Assuming an average delivery of 15,700 particles/mm^3 and loading of 0.5 mg doxorubicin per 10^{10} particles, we can realistically expect to deliver doxorubicin in the μM range (∼1.35μM) with a single administration of nanoparticles. While this number is still lower than what we estimate as IC_{50} for these cells, it appears that we are on the cusp of being able to able to achieve therapeutic benefit with our current generation of silicon-based drug delivery strategies.

In humans, doxorubicin is administered intravenously for a wide range of cancers. The amount of drug patients receive is carefully limited due to its toxicity. If we scale the current particle dosage scheme used in mice (∼7 mg/m^2/dose, assuming 0.5 mg doxorubicin loading per 10^{10} particles), we are well below typical doses used in humans (60-75 mg/m^2/dose). This would provide flexibility to inject a larger numbers of particles or to load higher quantities of drug. The ability of free doxorubicin to reach tumors is relatively poor, on the order of ≤0.1% of the injected dose per

gram organ (%ID/g). Recent advances in particle design now allow the delivery of particles above 1%ID/g,[36,37] suggesting that, it may be possible to deliver more drug to the tumor when using a clinically equivalent dose.

The silicon particle drug delivery platform offers many degrees-of-freedom for additional optimization. The ability to load free doxorubicin, for example, is limited by the surface area of the nanopores. Particle porosity may be modulated to increase the loading density,[46] or alternatively, doxorubicin may be encapsulated in liposomes and then loaded into the pores, a strategy which we have previously used for improving the loading density of siRNA.[39] The size, shape, and surface properties of these particles may be modulated to control their behavior within the bloodstream[37,47] and improve their ability to accumulate in tumors.[37] Additionally, the degradation of these particles can be controlled with the use of different capping agents[42] to create particles that release drugs at different rates.

Our work suggests the need for particles capable of sustained drug delivery. In the simulation, the therapeutic effect of doxorubicin-loaded nanoparticles is dependent on the doxorubicin release and diffusion kinetics. The time-scale of doxorubicin diffusion and uptake is significantly more rapid than cell death and removal, thus it is expected that drug levels after an initial burst release would be insufficient to induce death for cells farther removed from the vasculature.[48,49] For this reason, we simulated a continuous release of drug for 4 days. Interestingly, even with a continuous release model, tumor shrinkage begins to level off after several days after treatment. This behavior is attributed to heterogeneities in the tumor and vascular structures, which in turn limits doxorubicin transport. These heterogeneities are themselves dynamic, such that when cells undergo apoptosis, additional regions of poor drug penetration may be created. Simply delivering more nanoparticles or more drug per particle in a single injection may not necessarily be better; instead, this work suggests that smarter particles designed through a combination of mathematical modeling and empirical data collection may provide a more optimal treatment strategy.

The model may be extended to simulate a variety of initial drug concentrations and calibrated to various drugs and cell types, in order to predict the response for specific tumors. Such a database could be used to help determine an optimal drug/particle formulation (or a combination of formulations) to achieve tumor eradication. This is particularly important for poorly vascularized tumors, in which the IC_{50} may itself change as a function of time and location. In previous comparisons between cell monolayers and tumor spheroids *in vitro*, we found that the IC_{50} may increase by a factor ranging from 10 to 100 when transitioning from a 2-D system to an avascular 3-D system characterized by regions of poor diffusion.[7] We would expect the IC_{50} of poorly vascularized, heterogeneous tumors to fall somewhere between that of monolayer culture and avascular spheroids. Further joint IVM and modeling work would be needed to study and develop solutions to this challenge.

Our proposed integrated approach to modeling is expected to be instrumental in unraveling disease and drug mechanisms. This work could one day be used to quantitatively evaluate patient-specific tumor responses to nanotherapeutics in order to better understand discrepancies between predicted and actual treatment outcomes. The relative cost-effectiveness of this approach allows rapid, systematic investigation and optimization of treatment strategies. Rigorously validated and accurately calibrated models of nanotherapeutics drug delivery could provide a powerful "dry-lab" that complements traditional wet-labs for fundamental research, drug discovery, and patient treatment.[50] Findings could suggest routes of experimentation in the pursuit of new therapeutic strategies and targets. Strengths and weaknesses of the computational models could be uncovered and addressed in an iterative process of improvement and ever-increasing accuracy. This methodology has the potential to facilitate discovery and progress in the understanding and treatment cancer, and provide renewed hope to patients.

V. CONCLUSIONS

The modeling work presented here demonstrates how increasingly sophisticated modeling technology, driven by computational simulation and calibrated with experimental data, can be developed to provide an investigative tool complementary to traditional methods. Intravital microscopy is an ideal partner for this approach, capable of providing quantitative measurements of dynamic events

in vivo. This integrated approach is expected to offer insights into *in vivo* drug delivery, as well as help simulate the therapeutic effects of the delivery devices and refine their specifications for optimum efficacy with minimal side effects.

VI. MATERIALS AND METHODS

A. Silicon particle fabrication

Plateloid particles of 1000 nm diameter x 400 nm thickness were fabricated in the Microelectronics Research Center at The University of Texas at Austin using a combination of electrochemical etching and lithography as first described in.[46] Scanning electron microscopy (SEM) images of particles were acquired under high vacuum at 30 kV with a spot size of 3.0 using a FEI Quanta 400 FEG-ESEM (Hillsboro, OR). Additional fabrication and characterization information may be found in.[36] Particles were labeled with fluorescent dye molecules using a protocol modified from.[51] Briefly, the surface of oxidized particles was aminated using 1% (v/v) 3-aminopropyltriethoxysilane solution (APTES; Sigma-Aldrich) in 98% isopropanol (IPA; Sigma-Aldrich) for 30 minutes at 35°C. Aminated particles were washed twice in IPA, dried under vacuum overnight to polymerize the silane layer, and then reacted with 1mg/ml Alexa Fluor 555 succidymal ester (Invitrogen) suspended in dimethyl sulfoxide (DMSO; Sigma-Aldrich) containing 100mM triethanol amine (TEA; Sigma-Aldrich). Particles were prepared for injection by washing 5 times with phosphate buffered saline (PBS) and sonicating briefly immediately before injection.

B. Animal models

Melanoma tumors were generated in wild-type C57BL/6J mice (Charles River Laboratories, Wilmington, MA) by a one-time subcutaneous injection of 10^6 human B16 melanoma cells (ATCC, Manassas, VA) in the flank of wild-type mice. These cells recruit native vessels to form well-vascularized tumors whose growth rate directly relates to tumor vascularity.[52] When tumors reached 3-5 mm in diameter, they were exposed for intravital imaging using a skin-flap procedure. Mice received a one-time injection of fluorescently labeled autologous red blood cells (RBCs) 1-3 days prior to imaging, in order to allow visualization of blood flow dynamics. RBCs were collected retro-orbitally, stained with carbocyanine DiD (Invitrogen, Carlsbad, CA) at 37°C using the manufacturer's recommended protocol, and immediately re-injected behind the contralateral eye. Approximately 3-5% of the total RBCs were labeled per mouse. To delineate the vasculature, mice received an intravenous injection 40kDa FITC-dextran (1uM in PBS, Invitrogen) immediately prior to imaging. This was for illustrative purposes only and was not used for quantitative imaging experiments. All intravital animal protocols were reviewed and approved by the IACUC at The Methodist Hospital Research Institute.

C. Intravital microscopy

Live animals were imaged on an upright Nikon A1R laser scanning confocal microscope platform equipped with a resonance scanner, isoflurane anesthesia system, heated stage, and custom coverslip mounts. Bandpass filters of 30-50 nm width centered at 525 nm (488 ex; FITC-dextran), 595 nm (561 ex; particles), and 700 nm (640 ex; red blood cells). 512 x 512 bit three-channel images were acquired from a single organ per animal at 30 - 60 frames per second from the time of injection using high-NA, LWD objectives (4x, 20x, 40x) with a pinhole of 1.0 Airy units. To minimize local phototoxicity and compensate for tissue heterogeneity, randomly selected non-overlapping regions of interest were cycled through continuously for up to 15 minutes. Anesthetized mice were injected retro-orbitally with 5×10^8 particles in 50μl PBS and monitored for up to 3 hours. The retro-orbital route was chosen over tail-vein injection due to its accessibility and reproducibility for quantitative imaging experiments. Using this delivery route, particles are observed to reach well-vascularized tumors in approximately 15 seconds. Particle circulation and accumulation was quantified using Image J v1.45 (NIH) as described in.[36]

D. Mathematical model

The model describes viable and necrotic tumor tissue, diffusion of small molecules (cell substrates and drug), and conservation of mass and momentum, as detailed in.[35] Mass conservation equations describe growth (proliferation as a function of total cycling cells) and death from hypoxia (apoptosis as a function of oxygen) and from drug cytotoxicity (apoptosis as a function of cell sensitivity and cycling cells). These are combined with diffusion of small molecules to a reaction-diffusion equation. Rate constants for proliferation and apoptosis are modified by functions that represent their dependence on cell nutrients and oxygen (proliferation) and drug concentration (death), along with a dependence on spatial diffusion of these substances. Model parameters values are calibrated to intravital[36] as well as published experimental data as in.[6,7] We simulate the transport and drug release of large ($>$ 100 nm) porous silicon nanoparticles loaded with doxorubicin.

1. Tumor growth

Following,[22] we denote the tumor mass as Ω and denote its boundary as Σ. The tumor is divided into three regions: a proliferating region Ω_P where the tumor cells have sufficient levels of oxygen and cell nutrients for proliferation; a hypoxic region Ω_H where the oxygen and cell nutrient levels are sufficient for the cells to survive but not enough to sustain proliferation; a necrotic region Ω_N where the nutrient level is insufficient to maintain the cells alive. The non-dimensional tumor velocity is given by a generalized Darcy's law:[22]

$$\mathbf{v}_c = -\mu \nabla P + \chi_E \nabla E$$

where μ is the cell-mobility modeling the net effects of cell-cell and cell-matrix adhesion, P is the oncotic pressure, χ_E is the haptotaxis coefficient, and E is the ECM density (composed of a non-diffusible matrix macromolecule such as fibronectin or collagen). Details for χ_E and E are in.[22,35] We associate the growth of the tumor with the rate of volume change by assuming that the density of cells is constant in the proliferating region:

$$\nabla \cdot \mathbf{v}_c = \lambda_p$$

where λ_p is the non-dimensional net proliferation rate (see below).

2. Angiogenesis

To account for tumor-induced angiogenesis, we couple the tumor growth model with the angiogenesis model developed by McDougall *et al.*[19] that accounts for blood flow through the vascular network, non-Newtonian effects, vascular leakage and vascular network remodeling due to wall shear stress and mechanical stresses generated by the growing tumor. The architecture of the tumor vasculature is described in detail in.[22,35] The tumor cells are initially placed at the same distance from the surrounding vasculature, but as the tumor grows, this distance varies depending on the pressure that the vessels experience as a function of cell proliferation and death, as well as by the formation of new vessels through angiogenesis.

3. Transport of oxygen and drugs

We use a model[35] following previous work,[22] which describes the transport of small molecules s such as oxygen (s=σ) and drug (s=D) at the point of release from the vasculature by quasi-steady reaction-diffusion equations. We assume that the small molecules are supplied by the pre-existing vasculature as well as the neo-vasculature at rates λ^s_{pre} and λ^s_{neo}, respectively, diffuse into the host and cancerous tissue with a diffusion coefficient D_s, are uptaken both by the normal cells (with a rate λ^s_{tissue}) and tumor cells (λ^s_{tumor} in the proliferating region and q_s in the hypoxic region), and

decay (with a rate λ_N^s) in the necrotic regions. The equations are:

$$0 = \nabla \cdot (D_s \nabla s) - \lambda^s(s)s + \lambda_{ev}^s(\mathbf{x}, t, 1_{vessel}, p, s, h)$$

$$\lambda^s = \begin{cases} \lambda_{tissue}^s & outside\ \Omega \\ \lambda_{tumor}^s & in\ \Omega_P \\ q_s(s) & in\ \Omega_H \\ \lambda_N^s & in\ \Omega_N \end{cases}$$

where in general q_s is a smooth interpolating function, $\mathbf{x}$ is position in space, t is time, p is the tumor (solid) pressure, and h is the hematocrit in the neo-vascular network related to oxygen extravasation (following[22]). This extravasation is affected by the interstitial pressure p_i outside of the vessels scaled by the effective pressure p_e, with k_{p_i} representing the weight of the convective transport component of the small molecules:

$$\lambda_{ev}^{\sigma} = \bar{\lambda}_{ev}^{\sigma} \mathbf{1}_{vessel}(\mathbf{x}, t)(\frac{h}{\bar{H}_D} - \bar{h}_{min})^{+}(1 - k_{p_i}\frac{p_i}{p_e})(1 - \sigma)$$

$$\lambda_{ev}^{D} = \bar{\lambda}_{ev}^{D} \mathbf{1}_{vessel}(\mathbf{x}, t)(1 - k_{p_i}\frac{p_i}{p_e})(\frac{C^t}{\bar{C}_D} - \bar{C}_{min} - D)$$

where $\bar{\lambda}_{ev}^s$ is the constant transfer rate from the pre-existing and tumor-induced vessels, and $\mathbf{1}$ is the characteristic function of the vessels (i.e., $\mathbf{1}_{\mathrm{vessel}}$ equals 1 at the locations of the vessels and 0 otherwise). The constants $\bar{H}_D$ and h_{min} represent the normal blood hematocrit and the minimum hematocrit required for oxygen extravasation, respectively. We assume that the drug level in the particles attached to tumoral vessels begins as $\bar{C}_D$ and that $\bar{C}_{min}$ reflects the minimum value necessary for the drug to be released. This release is assumed to follow $C^t = \bar{C}_D e^{-\alpha t}$, where the decay α is estimated from the experiments. The boundary conditions for the diffusion equations are taken to be zero Neumann condition, $\frac{\partial D}{\partial n} = 0$.

4. Drug effect on the tumor

We assume the drug is effective only where the drug level is above a threshold T_{drug}, and that the drug only affects proliferating cells. For simplicity, we assume that death occurs immediately. We include the effect of drug into the proliferation termλ_p, where $\bar{\lambda}_{effect}$ is the rescaling factor in the unit of effect per drug concentration and $\bar{C}_D$ rescales the drug concentration D in the tissue:

$$\lambda_p = \begin{cases} 0 & outside\ \Omega \\ \sigma(1 - \bar{\lambda}_{effect}\bar{C}_D \mathbf{1}_{D>T_{drug}}) - A & in\ \Omega_p \\ 0 & in\ \Omega_H \\ -G_N & in\ \Omega_N \end{cases}$$

where A is the natural apoptosis rate and and G_N is the non-dimensional rate of volume loss in the necrotic regions assuming that fluid is removed and cellular debris is constantly degraded.

We run simulations to determine the initial concentration of drug, measured by $\bar{C}_D$, in order to achieve an average 50% tumor inhibition (the IC_{50} concentration) compared to a control tumor where no drug is applied during the same time. This defines the required load of drug per particle as well as the number of particles per volume needed to attain this inhibition.

ACKNOWLEDGMENTS

This work was supported in part by a NIH/NCI Physical Sciences – Oncology Center (PS-OC) Young Investigator Trans-Network Award to AV and HF as a part of the Methodist (U54CA143837) and USC (U54CA143907) PS-OC Centers. VC acknowledges funding by the Cullen Trust for Health Care, NIH/NCI PS-OC grant U54CA143837, NIH-ICBP grant U54CA149196, and NSF grant DMS-0818104. JL acknowledges funding by the NSF, Division of Mathematical Sciences, and NIH grant P50GM76516 for a Center of Excellence in Systems Biology at the University of California, Irvine. MF acknowledges funding by NIH/NCI PS-OC grant U54CA143837 and

additional research support from DoD/BCRP (W81XWH-09-1-0212), NIH/NCI (U54CA151668) and Ernest Cockrell Jr. Distinguished Endowed Chair.

[1] Franziska Michor, Jan Liphardt, Mauro Ferrari, and Jonathan Widom, "What does physics have to do with cancer?," Nature reviews **11**(9), 657-670 (2011).
[2] M. Ferrari, "Frontiers in cancer nanomedicine: directing mass transport through biological barriers," Trends Biotechnol **28**(4), 181-188 (2010).
[3] Rakesh K. Jain, "Transport of Molecules, Particles, and Cells in Solid Tumors," Annual Review of Biomedical Engineering **1**(1), 241-263 (1999).
[4] S. Nie, "Understanding and overcoming major barriers in cancer nanomedicine," Nanomedicine (Lond) **5**(4), 523-528 (2010).
[5] J. Sinek, H. Frieboes, X. Zheng, and V. Cristini, "Two-dimensional chemotherapy simulations demonstrate fundamental transport and tumor response limitations involving nanoparticles," Biomed Microdevices **6**(4), 297-309 (2004).
[6] J. P. Sinek, S. Sanga, X. Zheng, H. B. Frieboes, M. Ferrari, and V. Cristini, "Predicting drug pharmacokinetics and effect in vascularized tumors using computer simulation," J Math Biol **58**(4-5), 485-510 (2009).
[7] H. B. Frieboes, M. E. Edgerton, J. P. Fruehauf, F. R. Rose, L. K. Worrall, R. A. Gatenby, M. Ferrari, and V. Cristini, "Prediction of drug response in breast cancer using integrative experimental/computational modeling," Cancer Res **69**(10), 4484-4492 (2009).
[8] Helen M. Byrne, "Dissecting cancer through mathematics: from the cell to the animal model," Nature reviews **10**(3), 221-230 (2010).
[9] J. S. Lowengrub, H. B. Frieboes, F. Jin, Y. L. Chuang, X. Li, P. Macklin, S. M. Wise, and V. Cristini, "Nonlinear modelling of cancer: bridging the gap between cells and tumours," Nonlinearity **23**(1), R1-R9 (2010).
[10] I. M. van Leeuwen, C. M. Edwards, M. Ilyas, and H. M. Byrne, "Towards a multiscale model of colorectal cancer," World J Gastroenterol **13**(9), 1399-1407 (2007).
[11] Tiina Roose, S. Jonathan Chapman, and Philip K. Maini, "Mathematical Models of Avascular Tumor Growth," SIAM Rev. **49**(2), 179-208 (2007).
[12] Sergey Astanin and Luigi Preziosi, "Multiphase Models of Tumour Growth: Selected Topics in Cancer Modeling", (Birkhuser, Boston, 2008), pp. 1-31.
[13] H. L. Harpold, E. C. Alvord, Jr., and K. R. Swanson, "The evolution of mathematical modeling of glioma proliferation and invasion," J Neuropathol Exp Neurol **66**(1), 1-9 (2007).
[14] A. R. Anderson and V. Quaranta, "Integrative mathematical oncology," Nature reviews **8**(3), 227-234 (2008).
[15] T. S. Deisboeck, L. Zhang, J. Yoon, and J. Costa, "In silico cancer modeling: is it ready for prime time?," Nat Clin Pract Oncol **6**(1), 34-42 (2009).
[16] A. C. Ventura, T. L. Jackson, and S. D. Merajver, "On the role of cell signaling models in cancer research," Cancer Res **69**(2), 400-402 (2009).
[17] A. R. Anderson and M. A. Chaplain, "Continuous and discrete mathematical models of tumor-induced angiogenesis," Bull Math Biol **60**(5), 857-899 (1998).
[18] S. R. McDougall, A. R. Anderson, M. A. Chaplain, and J. A. Sherratt, "Mathematical modelling of flow through vascular networks: implications for tumour-induced angiogenesis and chemotherapy strategies," Bull Math Biol **64**(4), 673-702 (2002).
[19] S. R. McDougall, A. R. Anderson, and M. A. Chaplain, "Mathematical modelling of dynamic adaptive tumour-induced angiogenesis: clinical implications and therapeutic targeting strategies," J Theor Biol **241**(3), 564-589 (2006).
[20] A. Stéphanou, S. McDougall, A. Anderson, and M. A. J. Chaplain, "Mathematical modelling of the influence of blood rheological properties upon adaptive tumour-induced angiogenesis," Math Comput Model **44**, 96–123 (2006).
[21] M. R. Owen, T. Alarcon, P. K. Maini, and H. M. Byrne, "Angiogenesis and vascular remodelling in normal and cancerous tissues," J Math Biol **58**(4-5), 689-721 (2009).
[22] P. Macklin, S. McDougall, A. R. Anderson, M. A. Chaplain, V. Cristini, and J. Lowengrub, "Multiscale modelling and nonlinear simulation of vascular tumour growth," J Math Biol **58**(4-5), 765-798 (2009).
[23] T. L. Jackson, "Intracellular accumulation and mechanism of action of doxorubicin in a spatio-temporal tumor model," J Theor Biol **220**(2), 201-213 (2003).
[24] E. S. Norris, J. R. King, and H. M. Byrne, "Modelling the response of spatially structured tumours to chemotherapy: drug kinetics," Math Comput Model **43**, 820–837 (2006).
[25] H. Enderling, M. A. Chaplain, A. R. Anderson, and J. S. Vaidya, "A mathematical model of breast cancer development, local treatment and recurrence," J Theor Biol **246**(2), 245-259 (2007).
[26] V. Cristini, J. Lowengrub, and Q. Nie, "Nonlinear simulation of tumor growth," J Math Biol **46**(3), 191-224 (2003).
[27] V. Cristini, H. B. Frieboes, R. Gatenby, S. Caserta, M. Ferrari, and J. Sinek, "Morphologic instability and cancer invasion," Clin Cancer Res **11**(19 Pt 1), 6772-6779 (2005).
[28] H. B. Frieboes, X. Zheng, C. H. Sun, B. Tromberg, R. Gatenby, and V. Cristini, "An integrated computational/experimental model of tumor invasion," Cancer Res **66**(3), 1597-1604 (2006).
[29] H. B. Frieboes, J. S. Lowengrub, S. Wise, X. Zheng, P. Macklin, E. L. Bearer, and V. Cristini, "Computer simulation of glioma growth and morphology," Neuroimage **37 Suppl 1**, S59-70 (2007).
[30] H. B. Frieboes, F. Jin, Y. L. Chuang, S. M. Wise, J. S. Lowengrub, and V. Cristini, "Three-dimensional multispecies nonlinear tumor growth-II: Tumor invasion and angiogenesis," J Theor Biol **264**(4), 1254-1278 (2010).
[31] S. Sanga, J. P. Sinek, H. B. Frieboes, M. Ferrari, J. P. Fruehauf, and V. Cristini, "Mathematical modeling of cancer progression and response to chemotherapy," Expert Rev Anticancer Ther **6**(10), 1361-1376 (2006).

[32] A. R. Anderson, A. M. Weaver, P. T. Cummings, and V. Quaranta, "Tumor morphology and phenotypic evolution driven by selective pressure from the microenvironment," Cell **127**(5), 905-915 (2006).
[33] P. Macklin and J. S. Lowengrub, "Nonlinear simulation of the effect of microenvironment on tumor growth," J Theor Biol **245**, 677–704 (2007).
[34] X. Zheng, S. M. Wise, and V. Cristini, "Nonlinear simulation of tumor necrosis, neo-vascularization and tissue invasion via an adaptive finite-element/level-set method," Bull Math Biol **67**(2), 211-259 (2005).
[35] M. Wu, H. B. Frieboes, S. McDougall, M. A. Chaplain, V. Cristini, and J. Lowengrub, "The effect of interstitial pressure on tumor growth and transport of therapeutic agents: coupling with the blood and lymphatic vascular systems," (Submitted).
[36] A van de Ven, P. Kim, O. Haley, J. Fakhoury, G. Adriani, J. Schmulen, P. Moloney, F. Hussain, M. Ferrari, X. Liu, S. Yun, and P. Decuzzi, "Rapid tumoritropic accumulation of systemically injected plateloid particles and their biodistribution," JCR, In press. (2011).
[37] P. Decuzzi, B. Godin, T. Tanaka, S. Y. Lee, C. Chiappini, X. Liu, and M. Ferrari, "Size and shape effects in the biodistribution of intravascularly injected particles," J Control Release **141**(3), 320-327 (2010).
[38] Gu J., Godin B., Serda R. E., Ferrati S., Liu X., "Multistage mesoporous silicon-based nanocarriers: biocompatibility and controlled degradation in physiological fluids," *35th Annual Meeting & Exposition of the Controlled Release Society* **575** (New York City, New York) (2008).
[39] T. Tanaka, L. S. Mangala, P. E. Vivas-Mejia, R. Nieves-Alicea, A. P. Mann, E. Mora, H. D. Han, M. M. Shahzad, X. Liu, R. Bhavane, J. Gu, J. R. Fakhoury, C. Chiappini, C. Lu, K. Matsuo, B. Godin, R. L. Stone, A. M. Nick, G. Lopez-Berestein, A. K. Sood, and M. Ferrari, "Sustained small interfering RNA delivery by mesoporous silicon particles," Cancer Res **70**(9), 3687-3696 (2010).
[40] Huan Meng, Monty Liong, Tian Xia, Zongxi Li, Zhaoxia Ji, Jeffrey I. Zink, and Andre E. Nel, "Engineered Design of Mesoporous Silica Nanoparticles to Deliver Doxorubicin and P-Glycoprotein siRNA to Overcome Drug Resistance in a Cancer Cell Line," ACS Nano **4**(8), 4539-4550 (2010).
[41] Ji-Ho Park, Luo Gu, Geoffrey von Maltzahn, Erkki Ruoslahti, Sangeeta N. Bhatia, and Michael J. Sailor, "Biodegradable luminescent porous silicon nanoparticles for in vivo applications," Nat Mater **8**(4), 331-336 (2009).
[42] Biana Godin, Jianhua Gu, Rita E. Serda, Rohan Bhavane, Ennio Tasciotti, Ciro Chiappini, Xuewu Liu, Takemi Tanaka, Paolo Decuzzi, and Mauro Ferrari, "Tailoring the degradation kinetics of mesoporous silicon structures through PEGylation," Journal of Biomedical Materials Research Part A **94A**(4), 1236-1243 (2010).
[43] Joseph J. Casciari, Stratis V. Sotirchos, and Robert M. Sutherland, "Variations in tumor cell growth rates and metabolism with oxygen concentration, glucose concentration, and extracellular pH," Journal of Cellular Physiology **151**(2), 386-394 (1992).
[44] D. D. Sumner and J. T. Stevens, "Pharmacokinetic factors influencing risk assessment: saturation of biochemical processes and cofactor depletion," Environ Health Perspect **102 Suppl 11**, 13-22 (1994).
[45] R. Ganapathi, H. Schmidt, D. Grabowski, M. Melia, and N. Ratliff, "Modulation in vitro and in vivo of cytotoxicity but not cellular levels of doxorubicin by the calmodulin inhibitor trifluoperazine is dependent on the level of resistance," British journal of cancer **58**(3), 335-340 (1988).
[46] C. Chiappini, E. Tasciotti, J. R. Fakhoury, D. Fine, L. Pullan, Y. C. Wang, L. Fu, X. Liu, and M. Ferrari, "Tailored porous silicon microparticles: fabrication and properties," Chemphyschem **11**(5), 1029-1035 (2010).
[47] P. Decuzzi, R. Pasqualini, W. Arap, and M. Ferrari, "Intravascular delivery of particulate systems: does geometry really matter?," Pharm Res **26**(1), 235-243 (2009).
[48] J. Lankelma, H. Dekker, F. R. Luque, S. Luykx, K. Hoekman, P. van der Valk, P. J. van Diest, and H. M. Pinedo, "Doxorubicin gradients in human breast cancer," Clin Cancer Res **5**(7), 1703-1707 (1999).
[49] A. J. Primeau, A. Rendon, D. Hedley, L. Lilge, and I. F. Tannock, "The distribution of the anticancer drug Doxorubicin in relation to blood vessels in solid tumors," Clin Cancer Res **11**(24 Pt 1), 8782-8788 (2005).
[50] M. Ferrari, "Cancer nanotechnology: opportunities and challenges," Nature reviews **5**(3), 161-171 (2005).
[51] R. E. Serda, A. Mack, A. L. van de Ven, S. Ferrati, K. Dunner, Jr., B. Godin, C. Chiappini, M. Landry, L. Brousseau, X. Liu, A. J. Bean, and M. Ferrari, "Logic-embedded vectors for intracellular partitioning, endosomal escape, and exocytosis of nanoparticles," Small **6**(23), 2691-2700 (2010).
[52] M. Gutman, R. K. Singh, S. Yoon, K. Xie, C. D. Bucana, and I. J. Fidler, "Leukocyte-induced angiogenesis and subcutaneous growth of B16 melanoma," Cancer Biother **9**(2), 163-170 (1994).